RAPID COAL DEVOLATILIZATION IN A RADIANT COAL FLOW REACTOR

John Chen, Y. Cleo Chang, and Stephen Niksa
High Temperature Gasdynamics Laboratory
Mechanical Engineering Department
Stanford University
Stanford, CA 94305

INTRODUCTION

Determinations of the product distributions from coal devolatilization under simulated pulverized fuel (p.f.) firing will enable better descriptions of the heat release, pollutant formation, sooting, and the evolution of polycyclic aromatic compounds (PAC). While these connections are widely recognized, only a handful of product distributions from very rapid coal devolatilization have been reported. Moreover, most of the available data was taken in entrained flow reactors, in which the time-temperature histories are obscured by mixing between preheated gases and the cold coal suspension at the injector as, for example, in Nenniger's study.[1] Also, since entrained process streams are very hot, the product distributions from primary devolatilization are significantly altered by secondary homogeneous chemistry.[2]

In this study, we introduce a novel radiant coal flow reactor which eliminates mixing and minimizes the extent of secondary chemistry. This system relies upon radiant heating of a thin coal suspension entrained into a stable, one-dimensional flow field. This furnace configuration is supported by rapid quenching to resolve reaction times on a scale of several milliseconds, aerodynamic segregation of particulate, aerosol, and gaseous products, and a battery of chemical analyses. Transient weight loss, tar yields, elemental compositions of the condensed products, and tar molecular weight distributions (MWDs) are reported for an Illinois #6, HVA bituminous coal. These results depict the devolatilization behavior at atmospheric pressure for particle residence times to 130 msec., furnace temperatures from 1000 to 1850K, heating rates exceeding 10^4K/s, and suspension loadings to 2400 particles/cm^3.

EXPERIMENTAL

Overview and Performance Characteristics

A schematic of the radiant coal flow devolatilization experiment appears in Fig. 1. At the top of the system, a feeder delivers fuel particles into an argon entrainment stream, forming an optically-thin suspension which flows downward into a radiant furnace section. The radiant section consists of a quartz tube situated on the axis of an inductively-heated graphite cylinder. Near-blackbody thermal emission from the graphite rapidly heats the particles as they traverse the furnace. Note that since the suspension is optically thin, the radiant heat flux is uniform, and that no mixing with a preheated gas stream is involved. Also, since the argon is transparent to the radiation, the gas remains relatively cool, thereby minimizing secondary reactions among the volatiles. Even though suspension loadings up to several thousand particles per cubic centimeter are maintained, the behavior in this system can be interpreted in terms of single-particle phenomena because the interparticle separation is at least ten particle diameters.

A schematic of the induction furnace section appears in Fig. 2. It consists of a 10 cm I. D., 5 cm long graphite cylinder encased in zirconium-oxide insulation which is wrapped by four turns of a water-cooled, copper induction coil. This assembly is mounted within water-cooled copper plates and a quartz housing. The overall height of the furnace is 9.5 cm. The graphite is heated inductively by a 10 kW, 450 kHz power supply. Wall temperatures are monitored with a disappearing filament pyrometer sighted onto the graphite through a small hole in the insulation to an uncertainty of 20K. In characterization studies with two-color pyrometry, axial temperature profiles within the graphite enclosure are uniform to within 98% of the mean temperature, except for the outermost 5 mm at both ends, over which the temperature falls to about 75% of the mean value.

The coal suspension enters the 22 mm O. D. quartz tube located on the axis of the furnace from a 10 mm tube, and is stabilized by a co-flowing, argon sheath flow. The relative flowrates of

the entrainment and sheath flows are set to minimize the extent of particle dispersion over the length of the furnace. They are not matched; rather, the conditions which yielded a uniform, pencil-like flow of coal over the furnace length at each gas velocity in cold-flow visualization studies are implemented in the experiments. Also, the suspension loadings reported here are based on the cross section of the entrainment stream only, the calculated slip velocity of the particles, and the calibrated coal feedrate.

Time resolution is achieved by varying the gas transit time from the furnace inlet to an argon quench nozzle mounted near the outlet of the radiant section. The reported residence times are based on direct measurements under experimental conditions. Residence times are assigned as the time interval between the interruption of two HeNe laser beams by the leading edge of a long pulse of fuel suspension. The two beams are separated by 11 cm, and placed as close to the inlet and outlet of the furnace as possible; nevertheless, this configuration does not necessarily contain the entire length of the active radiant zone.

The pyrolysis products are segregated into char particles, tar aerosol, and noncondensible gases using virtual impaction in an aerodynamic classifier, which is sketched in Fig. 3. All of the condensed phase products (char and tar) are recovered, and the coal feedrate is stable and reproducible, so that their respective yields can be assigned gravimetrically. At the inlet, the cooled process stream contains char particles, tar aerosol, and noncondensible gases at low levels in an argon stream. Following Nenninger's[4] design guidelines, the inlet jet is turbulent (Re_j = 7000), and the jet diameters and spacings are set at prescribed ratios. Most of the inlet gas stream is diverted radially outward into the annulus while a small portion passes through the central nozzle. This split is maintained by valves downstream of the impactor. Particles with sufficient inertia, viz. char particles, pass through this virtual impaction surface and into a wire mesh basket. Nominal sizes for the tar aerosol are only a few microns, while the char particles are at least 50 microns, so the separation efficiency is very high. For 50 micron coal particles, the separation efficiency into the mesh basket exceeded 97% in characterization studies, so that carry-over of char into the annulus is negligible.

A small portion of the inlet gas stream, typically 5%, passes through the lower nozzle, while the remainder of the flow convects the aerosol products into the annulus, where they deposit onto a four-stage assembly of glass fiber filters. Even though no tars could penetrate a single filter element, multiple stages are needed to manage the increasing pressure drop as the tars accumulate. The top three stages are punctured to decrease their flow resistance; nevertheless, most of the tar deposits onto these stages. The final stage scavenges the stream at the size threshold of the filters at 0.3 microns. Small amounts of aerosol also deposit onto the impactor wall, so this surface is isolated with a polypropylene liner, and such deposits are included in the reported aerosol yields.

Pure tar samples for subsequent chemical analyses are prepared by extraction with tetrahydrofuran (THF) in an ultrasonic bath, and filtration through a 0.5 micron Teflon membrane; any residue is weighed and denoted as the soot yield. The tar solution is concentrated before the remaining solvent is evaporated, following a procedure developed by Lafleur et al.[5]

Elemental compositions of the char and tar are measured with a Control Equipment 240X analyzer. Tar MWDs are based on gel-permeation chromatography in a Hewlett-Packard HP-1090 HPLC using three μStyragel columns (500Å and two 100Å) in series and broadband diode-array detection (212 to 400 nm). We adapted the calibration introduced by Rogers et al.[8] to diode-array detection using model compounds with molecular weights from 128 to 950; H/C ratios from 0.5 to 1.09; and proton aromaticities from 0.25 to 1. The calibration equation is:

$$\ln (\mathbf{MW}*(H/C)^{-0.0189}) = 10.7339 - 0.7611*\ln H_a + (-0.2202-0.0726*(\ln H/C))*V$$

where **MW** = Molecular weight
H/C = Hydrogen to carbon atomic ratio
H_a = Proton aromaticity, aromatic/(aromatic+aliphatic protons)
V = Retention volume, retention time*flow rate

Proton distributions are determined by ^1H NMR with a Varian XL-400 spectrometer operating at 400 MHz and are interpreted with tabulated chemical shifts.[9]

Coal Characteristics

The coal in these experiments is an Illinois #6, HVA bituminous coal (PSOC 1493D) obtained from the Pittsburgh Energy Technology Center (PETC). The ultimate and proximate analyses as reported by PETC are listed in Table I. The measured weight loss is converted to the dry, ash-free (daf) basis using the high-temperature ash value provided by PETC. These samples are aerodynamically classified, and two nominal size fractions are examined: 45-63 and 75-106 microns. All coal samples are dried at 60°C under vacuum for at least 12 hours and stored under argon.

RESULTS

Transient Devolatilization Behavior

The results in this section depict the influences of residence time and furnace wall temperature on the devolatilization behavior of the 75-106 micron sample. All of the results which follow are recorded at a reactor pressure a few inches of water above atmospheric, and a suspension loading of 400 particles/cm^3. The volatiles yields as a function of the reactor wall temperature at average inlet gas velocities of 0.25, 0.67, and 2.0 m/s appear in Fig. 4. For a fixed inlet gas velocity, residence times at different wall temperatures will vary because the acceleration due to the changing gas density is significant.

As expected, the onset of devolatilization shifts to higher wall temperatures as the gas velocity is increased, going from 1450K at 0.25 m/s to 1800K at 2.0 m/s. For velocities greater than 0.67 m/s, the available residence times are insufficient to achieve complete devolatilization at even the highest wall temperature, indicating that the particle temperature at the furnace outlet is substantially lower than the wall temperature. But at 0.25 m/s, the ultimate yield of 56 wt% is observed at a wall temperature of 1840K. This value is significantly greater than the proximate volatile matter, as expected for these conditions of rapid heating. Also at 0.25 m/s, devolatilization commences at a wall temperature of 1500K and the product evolution rates increase rapidly for higher wall temperatures. Note that replicate runs in the study are generally reproducible to within 2 wt%.

The aerosol yields at a gas velocity of 0.25 m/s is shown with the corresponding total weight loss in Fig. 5. The aerosol yield becomes significant at 1600K and increases monotonically with temperature up to the maximum yield at 1840K, which constitutes 42% of the total volatiles yield. While the ultimate proportion of tar is consistent with expectations for atmospheric pyrolysis of HVA bituminous coals, the relatively small amount of tar at lower temperatures is surprising. For HVA Pittsburgh seam bituminous coals, the initial proportions of tar to noncondensible gases are typically 10:1 (but in studies at lower heating rates[6,7]), while these proportions are inverted for this Illinois #6 coal. The tar samples from these conditions were analyzed for soot, but negligible amounts were observed in all cases. This observation strongly corroborates the absence of secondary homogeneous chemistry in this system, since pyrolysis tars rapidly convert to soot at temperatures above 1450K.[2]

The next study examines variations in residence time, which are measured at selected wall temperatures to characterize the kinetics of mass loss and tar evolution; results appear in Fig. 6 for wall temperatures of 1570, 1680, and 1840K. Although the wall temperatures are fixed in these studies, particle temperatures are increasing exponentially with increasing residence times, and probably never achieve the wall temperature in the available furnace length.

The onset of devolatilization shifts to shorter residence times as the wall temperature is increased, as expected. The complete transient evolution is evident only at 1840K, and shows two distinct stages of product evolution which are delineated by a distinct surge in the evolution rate between 72 and 77 msec. As seen above in Fig. 5, the proportions of tar to noncondensibles are surprisingly low during the initial stages of product formation. The transient data at 1840K also show that tar evolution ceases long before the ultimate yield is achieved, as seen in the behavior of HVA bituminous coals at slower heating rates. The fraction of soot in the aerosols is again found to be negligible for all conditions. Although they do not cover the entire approach to ultimate yields, the transient yields at 1680 and 1570K reliably convey the onset of devolatilization, and the relatively small amount of tar formed during the initial stages.

The proportions of carbon, hydrogen, and nitrogen (CHN) in the char and tar for various residence times at 1840K appear in Fig. 7. Note that all values are normalized by the distributions in the parent coal as reported by PETC, and that the error bars represent the range of measured values for replicate cases. Carbon and nitrogen contents of the chars (Fig. 7a) remain the same throughout devolatilization, but the hydrogen content falls monotically during product evolution. The corresponding elemental distributions for the tar aerosols in Fig. 7b are markedly insensitive to residence time and, hence, the extent of devolatilization. The carbon content of the aerosols closely resembles the parent coal's, but the tars are deficient in nitrogen, especially for tar collected during the earliest stages of devolatilization. As expected from the decreasing hydrogen content of the chars, the tars are uniformly enriched in hydrogen by about 40%.

Molecular weight distributions of tar generated at 66 msec. and 1840K (Fig.6) are shown in Fig. 8. These distibutions are partially integrated to depict the mass or mole fractions within 100 g/g-mole of the values on the abcissa. All tar samples have similar shapes with respect to the shoulders in the distributions. They do differ with extent of devolatilization, however, in both average molecular weights and proton aromaticity as shown in Table II for the tars generated at 1840K. With increasing residence time, hence, extent of devolatilization, the average molecular weight and proton aromaticities increase monotonically.

The Influence of Particle Size

In the next study, the nominal particle size was reduced to 50 microns, while the suspension loading was increased by a factor of six to 2400 particles/cm^3. The temperature dependence of weight loss and tar yields at constant inlet gas velocity (1.0 and 0.25 m/s) appear in Fig. 9. Note the similarities to the features in Figs. 4 and 5 for the larger sizes at lower loading, especially at a gas velocity of 0.25 m/s. The data are virtually identical for these two cases, for both weight loss and aerosol yields. This agreement may seem counterintuitive in that these studies involve stages of transient heating and the heating rates, being inversely proportional to size, should be higher for the smaller sizes. So higher yields at lower temperatures could have been expected for the smaller sizes, but are not observed.

In conventional entrained flow systems, increasing the suspension loading decreases the aggregate convective heat flux because of poorer mixing and the higher thermal capacitance of the suspension, so thermal transients extend over longer times; i. e., heating rates are lower for denser suspensions, all else the same. But the radiant furnace behaves differently. Since the suspensions remain optically thin at even the highest loadings of interest, the radiant flux is independent of loading. But the convective losses from the suspension increase with increasing surface area, and, consequently, with increasing loadings. Consequently, higher loadings increase the heating rate of the gases, so that the gas temperature more closely tracks the increasing temperature of the suspension. In summary, in this experiment the heating rates of the suspension and of the entrainment gas increase as the loading is increased.

This argument explains the agreement among the data in Figs. 5 and 9, in so far as the higher loading would tend to increase the gas temperature, while the smaller size would tend to decrease the suspension temperature. Apparently, these two factors are compensating, although temperature measurements are needed to demonstrate this. Note that arguments which invoke interparticle interactions seem implausible because the minimum interparticle spacing is at least 12 diameters for the cases in Fig. 9.

Discussion

In the radiant coal flow experiment, the thermal history of the fuel particles is not complicated by mixing between hot gases and cold suspensions, which will enable more reliable determinations of the fuel's time-temperature history. Since secondary chemistry among the volatiles is minimized in this system, detailed characterizations of the product distributions from pyrolysis at very rapid heating rates are also feasible.

Weight loss and tar aerosol yields from an Illinois #6 HVA bituminous coal were recorded for furnace temperatures to 1850K and residence times to 130 msec. for two different size-cuts of coal. Qualitatively, the transient data and elemental compositions of the condensed products exhibit

several interesting features, particularly (1) a distinct surge in the devolatilization rate midway through the process; (2) surprisingly low proportions of tar (for an HVA bituminous coal) during the first stage of product evolution; and (3) a shift to higher average molecular weight and proton aromaticity with increasing weight loss.

While these data reliably convey the experimental uncertainties and operating domain of this experiment, they are not yet suitable for rate determinations or model validation studies. The fuel's thermal histories are particularly uncertain, and both models and diagnostics are now being developed to assign the particle and gas temperatures. Also, the impact on the devolatilization behavior of the short unheated length of flow tube from the furnace outlet to the quench point and the effectiveness of the argon quench have not been assessed.

Acknowledgement

We are happy to acknowledge funding for this work from the Exploratory Research Program of the Electric Power Research Institute and, for John Chen, a fellowship from the Link Foundation for partial financial support.

References

1. Nenniger, R.D., Howard, J.B., and Sarofim, A.F.: Proceedings from the 1983 International Conference on Coal Science, IEA, Pittsburgh, 1983, pp.521-524.
2. Wornat, M.J.: *Pyrolysis-Induced Changes in the Composition of Polycyclic Aromatic Compounds from a Bituminous Coal*, Sc.D. thesis, Department of Chemical Engineering, MIT, 1988.
3. Ballantyne, A., Chou, H., Neoh, K., Orozco, N., and Stickler, D.: Final Report prepared for the U. S. DOE, Pittsburgh Energy Technology Center, Contract No. DE-AC22-84PC30291, October 1983.
4. Nenniger, R.D.: *Aerosols Produced from Coal Pyrolysis*, Sc.D. thesis, Department of Chemical Engineering, MIT, 1986.
5. Lafleur, A.L., Monchamp, P.A., Plummer, and E.F., Kruzel, E.L.: Analytical Letters **19** (21 & 22), 2103 (1986).
6. Oh, M.S.: *Softening Coal Pyrolysis*, Sc.D. thesis, Department of Chemical Engineering, MIT, 1985.
7. Bautista, J.R., Russel, W.B., and Saville, D.A.: Ind. Engr. Chem. Fundam. **25**, 536, 1986.
8. Rogers, P.A., Creagh, A.L., Prange, M.M., and Prausnitz, J.M.: Ind. Engr. Chem. Res. **26**, 2312-2318, 1987.
9. Collin, P.J., Tyler, R.J., and Wilson, M.A.: Fuel **59**, 479-486, 1980.

Size (Microns)	Volatile Matter	Moisture Free Weight Percent Ash	C	H	N	O	S
75 - 106	37.5	13.5	68.3	4.6	1.3	7.4	4.9
45 - 63	38.9	14.6	66.0	4.6	1.3	7.6	6.0

Table I: Proximate and Ultimate Analyses for Illinois #6, PSOC 1493D

Residence Time (ms)	Wt. Avg. M_w	No. Avg. M_n	Aromaticity H_a
66	706	501	0.28
72	807	557	0.28
77	813	556	0.29
87	834	568	0.33

Table II: Molecular Weight and Aromaticity of Tars Produced at 1840K

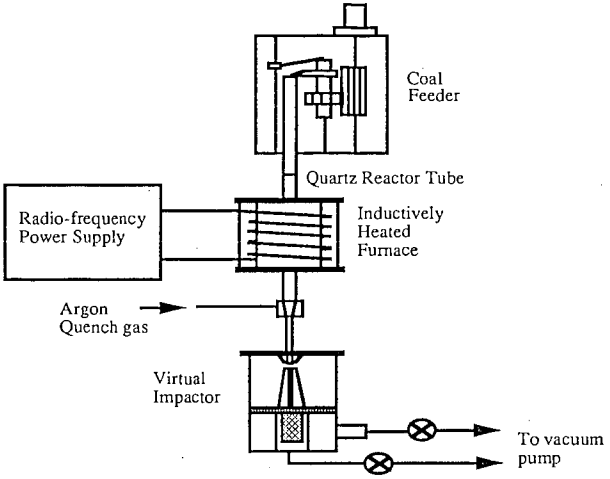

Fig. 1: The Radiant Coal Flow Reactor

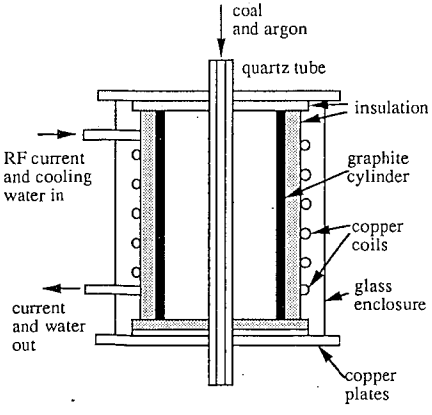

Fig. 2: The Inductively-Heated Furnace

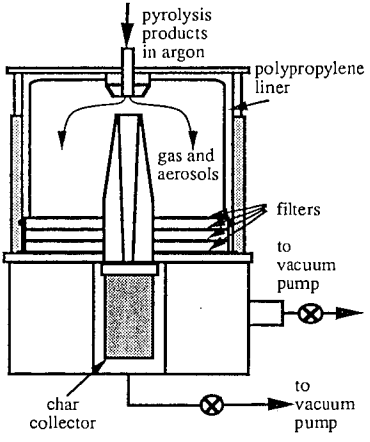

Figure 3: Schematic of the Virtual Impactor.

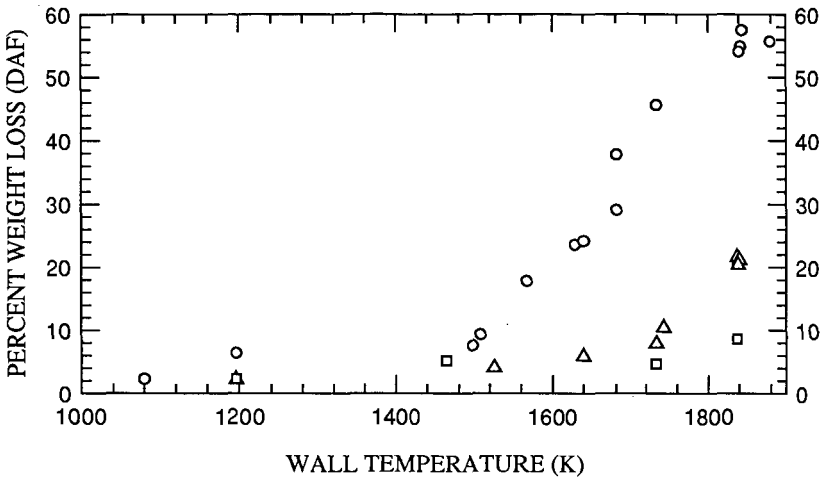

Fig. 4: Dry, ash-free weight loss for Illinois #6 coal, 75-106 μm, ○ 0.25 m/s, △ 0.67 m/s, □ 2.0 m/s inlet gas velocity, 400 particles/cc.

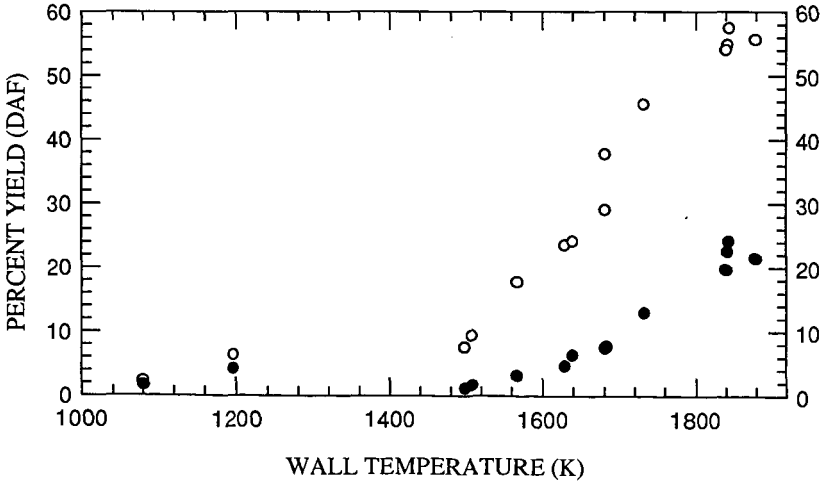

Fig. 5: Weight loss (OPEN symbols) and aerosol yield (FILLED symbols) for Illinois #6 coal, 75-106 μm particles, 0.25 m/s inlet gas velocity, 400 particles/cc.

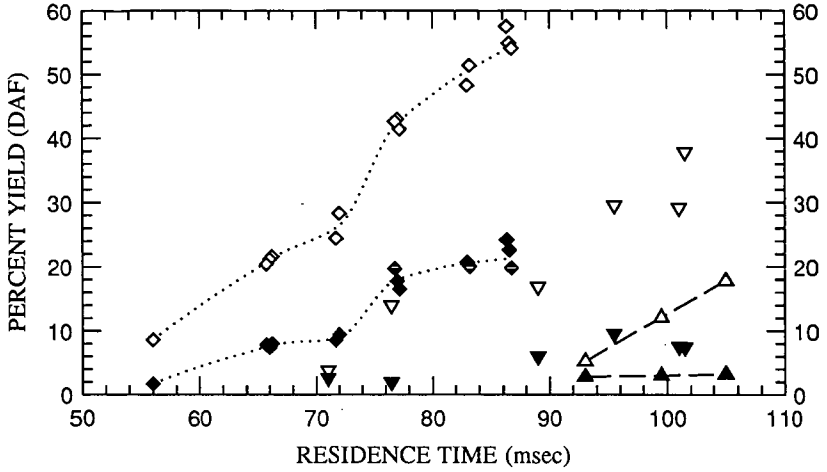

Fig. 6: Total (OPEN symbols) and aerosol yield (FILLED symbols) for Illinois #6 coal, 75-106 μm, ◇ 1840, ▽ 1680, △ 1570 K wall temperature, 400 particles/cc.

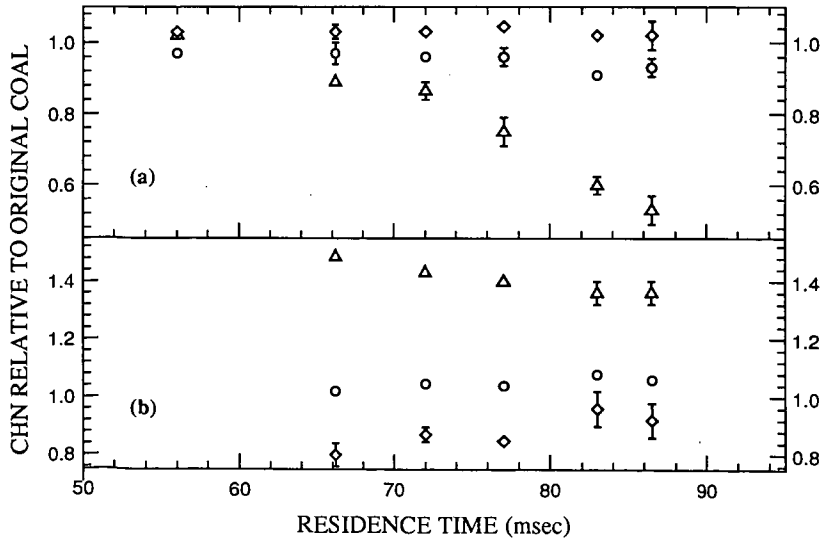

Fig. 7: Elemental composition of chars(a) and tars(b) for Illinois #6 coal, 75-106 μm, ○ carbon, △ hydrogen, ◇ nitrogen, T_w=1840 K, 400 particles/cc.

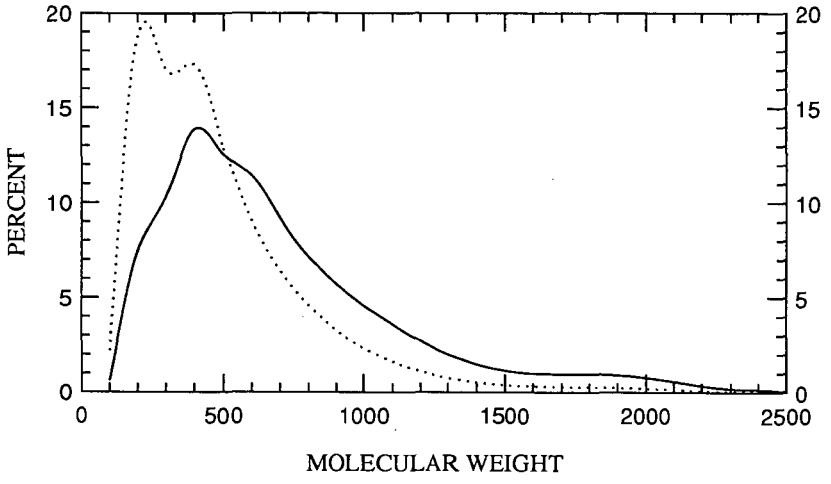

Figure 8: Molecular weight distributions of tar from Fig. 6 at 66 msec. and 1840K.
——— weight-average distribution, ····· number-average distribution.

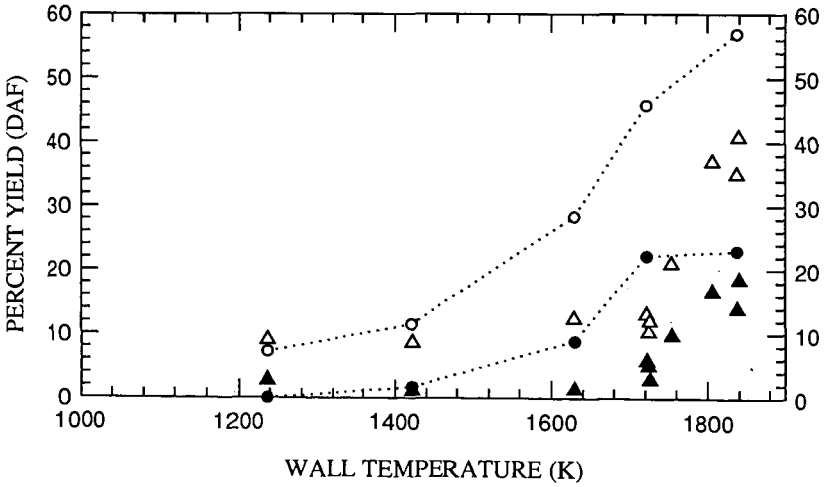

Fig. 9: Total (OPEN symbols) and aerosol yield (FILLED symbols) for 45-63 μm particles o 0.25 m/s, Δ 1.0 m/s inlet gas velocity, 2400 particles/cc.